Multifluid description of astrophysical and space plasmas
- Part 2 -

Daniel Gómez[1,2]

universidad de buenos aires - exactas
departamento de física
Juan José Giambiagi

IAFE
CONICET
UBA

(1) Departamento de Física, Fac. Cs. Exactas y Naturales, UBA, Argentina
(2) Instituto de Astronomía y Física del Espacio, UBA-CONICET, Argentina

Small scales: two-fluid equations

➡ The dimensionless version, for a length scale L_0 , density n_0 and Alfven speed $v_A = B_0 / \sqrt{4\pi m_i n_0}$

$$\frac{d\vec{U}_i}{dt} = \frac{1}{\varepsilon}(\vec{E} + \vec{U}_i \times \vec{B}) - \frac{\beta}{n}\vec{\nabla}p_i - \frac{\eta}{\varepsilon n}\vec{J}$$

$$\frac{m_e}{m_i}\frac{d\vec{U}_e}{dt} = -\frac{1}{\varepsilon}(\vec{E} + \vec{U}_e \times \vec{B}) - \frac{\beta}{n}\vec{\nabla}p_e + \frac{\eta}{\varepsilon n}\vec{J}$$

where $\vec{J} = \vec{\nabla} \times \vec{B} = \frac{n}{\varepsilon}(\vec{U}_i - \vec{U}_e)$

➡ We define the Hall parameter $\varepsilon = \frac{c}{\omega_{pi} L_0}$

as well as the plasma *beta* $\beta = \frac{p_0}{m_i n_0 v_A^2}$ and the electric resistivity $\eta = \frac{c^2 \nu_{ie}}{\omega_{pi}^2 L_0 v_A}$

➡ Adding these two equations yields:

$$\frac{d\vec{U}}{dt} = (\vec{\nabla} \times \vec{B}) \times (\vec{B} + \varepsilon_e^2 \vec{\nabla} \times \vec{J}) - \vec{\nabla}p$$

where $\vec{U} = \frac{m_i \vec{U}_i + m_e \vec{U}_e}{m_i + m_e}$

$$\varepsilon_e = \sqrt{\frac{m_e}{m_i}}\,\varepsilon = \frac{c}{\omega_{pe} L_0}$$

and $p = p_i + p_e$

Generalized Ohm's law

- Note that the equation of motion for electrons is also Ohm's law

$$\mu \frac{d\vec{U}_e}{dt} = -\frac{1}{\epsilon}(\vec{E} + \vec{U}_e \times \vec{B}) - \frac{\beta}{n}\vec{\nabla} p_e + \frac{\eta}{n\epsilon}\vec{J} \qquad \text{where} \qquad \mu = \frac{m_e}{m_i} \ll 1$$

- Considering that

$$\vec{U} = \frac{m_e \vec{U}_e + m_i \vec{U}_i}{m_e + m_i}$$

$$\vec{J} = n(\vec{U}_i - \vec{U}_e)$$

$$n = 1 \quad \text{(incompressible)}$$

$$\Rightarrow \quad \vec{U}_i = \vec{U} + \mu\epsilon\vec{J}$$

$$\vec{U}_e = \vec{U} - (1-\mu)\epsilon\vec{J}$$

- In the limit of massless electrons (i.e. $\mu \rightarrow 0$)

$$0 = -(\vec{E} + (\vec{U} - \epsilon\vec{J}) \times \vec{B}) - \beta\epsilon\vec{\nabla} p_e + \eta\vec{J}$$

also known as the generalized Ohm's law

- At large scales, much larger than the ion inertial length (i.e. $\epsilon \rightarrow 0$), it reduces to

$$E + \vec{U} \times \vec{B} = \eta\vec{J}$$

Ideal invariants in multi-fluid plasmas

➡ For each species s in the incompressible and ideal limit

$$m_s n_s \left(\partial_t \vec{U}_s - \vec{U}_s \times \vec{W}_s\right) = q_s n_s (\vec{E} + \frac{1}{c}\vec{U}_s \times \vec{B}) - \vec{\nabla}(p_s + m_s n_s \frac{U_s^2}{2})$$

➡ Using that $\vec{J} = \frac{c}{4\pi}\vec{\nabla} \times \vec{B} = \sum_s q_s n_s \vec{U}_s$ and $E = -\frac{1}{c}\partial_t \vec{A} - \vec{\nabla}\phi$

we can readily show that energy is an ideal invariant, where

$$E = \int d^3 r \left(\sum_s m_s n_s \frac{U_s^2}{2} + \frac{B^2}{8\Pi} \right)$$

➡ We also have a helicity per species which is conserved, where

$$H_s = \int d^3 r \left(\vec{A} + \frac{c m_s}{q_s}\vec{U}_s \right) \bullet \left(\vec{B} + \frac{c m_s}{q_s}\vec{W}_s \right)$$

Normal modes in 2F-HMHD

➡ If we linearize our equations around an equilibrium characterized by a uniform magnetic field we obtain, in the incompresible case, the following dispersion relation:

$$\left(\frac{\omega}{\vec{k}\bullet\vec{B}_0}\right)^2 \pm \frac{k\varepsilon}{1+\varepsilon_e^2 k^2}\left(\frac{\omega}{\vec{k}\bullet\vec{B}_0}\right) - \frac{1}{1+\varepsilon_e^2 k^2} = 0$$

➡ Asymptotically, at very large k, we have two branches

$$\omega \xrightarrow[k\to\infty]{} \omega_{ce}\cos\theta$$

$$\omega \xrightarrow[k\to\infty]{} \omega_{ci}\cos\theta$$

while for very small k, both branches simply become Alfven modes, i.e.

$$\omega \xrightarrow[k\to 0]{} k\cos\theta$$

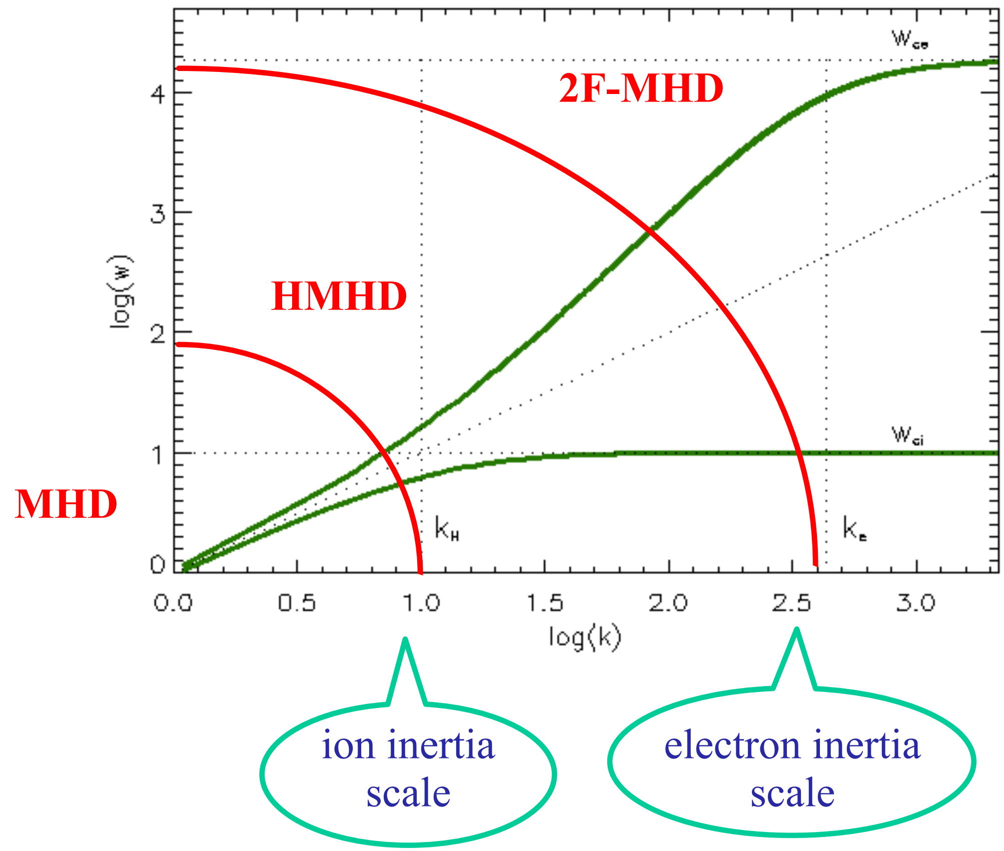

➡ Different approximations, just as one-fluid MHD, Hall-MHD and electron-inertia MHD can clearly be identified in this diagram.

Some applications

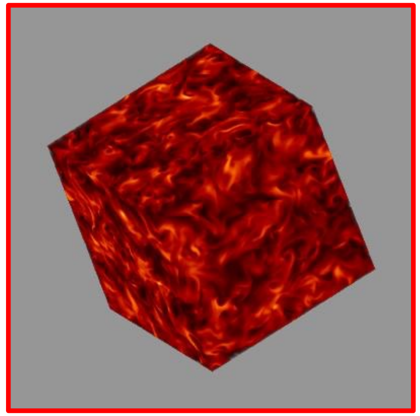

MHD

RMHD heating of solar coronal loops (Dmitruk & Gomez 1997, 1999)

Kelvin-Helmholtz instability in the solar corona (Gomez, DeLuca & Mininni 2016)

Hall-MHD

3D HMHD turbulent dynamos. (Mininni, Gomez & Mahajan 2003, 2005; Gomez, Dmitruk & Mininni 2010)

2.5 D HMHD reconnection at Earth magnetopause (Morales, Dasso & Gomez 2005, 2006)

RHMHD turbulence in the solar wind (Martin, Dmitruk & Gomez 2010, 2012)

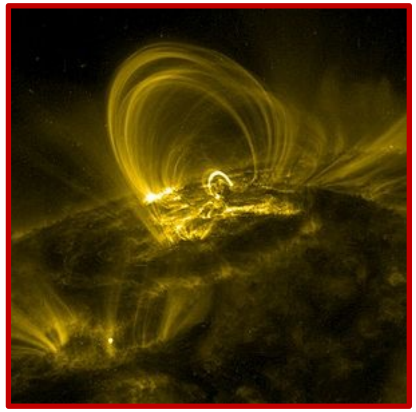

Hall MRI in accretion disks (Bejarano, Gomez & Brandenburg 2011)

Electron inertia

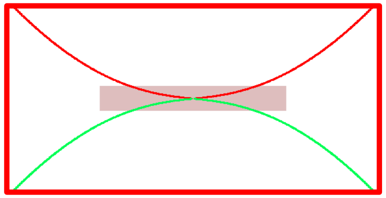

1D model of perpendicular shocks (Gomez et al. 2021).

Two-fluid turbulence in the solar wind (Andres et al. 2014, 2016).

Fast reconnection in 2.5 D (Andres, Dmitruk & Gomez 2014, 2016).

Retaining electron inertia

➡ In the equation for electrons (assuming incompressibility)

$$\frac{m_e}{m_i}\frac{d\vec{U}_e}{dt} = -\frac{1}{\varepsilon}(\vec{E} + \vec{U}_e \times \vec{B}) - \beta_e \vec{\nabla} p_e + \frac{\eta}{\varepsilon}\vec{J} \qquad \vec{J} = \vec{\nabla} \times \vec{B} = \frac{1}{\varepsilon}(\vec{U}_i - \vec{U}_e)$$

we replace $\vec{E} = -\frac{1}{c}\frac{\partial \vec{A}}{\partial t} - \vec{\nabla}\phi$ *and* $\vec{B} = \vec{\nabla} \times \vec{A}$

to obtain the following generalized induction equation (Andrés et al. 2014ab, PoP)

$$\frac{\partial}{\partial t}\vec{B}' = \vec{\nabla} \times \left[(\vec{U} - \varepsilon\vec{J}) \times \vec{B}' \right] + \eta \nabla^2 \vec{B} \quad , \qquad \vec{B}' = \vec{B} - \varepsilon_e^2 \nabla^2 \vec{B} - \frac{\varepsilon_e^2}{\varepsilon}\vec{\omega}$$

➡ See also Abdelhamid, Lingam & Mahajan 2016 for extended MHD.

➡ Electron inertia is quantified by the dimensionless parameter $\varepsilon_e = \sqrt{\frac{m_e}{m_i}}\,\varepsilon = \frac{c}{\omega_{pe} L_0}$

➡ Just as the Hall effect introduces the new spatial scale $k_H = \frac{1}{\varepsilon}$ (the ion skin depth), electron inertia introduces the electron skin depth $k_e = \frac{1}{\varepsilon_e}$ which satisfies

$$k_e = \sqrt{\frac{m_i}{m_e}}\, k_H >> k_H$$

Shocks in Space & in Astrophysics

- Shocks are an important source of heating and compression in space and astrophysical plasmas. Also, shocks are an important source of particle acceleration.

- For instance, shocks are formed during supernova explosions, when the stellar material propagates supersonically in the interstellar medium. Or when the solar wind impacts on each planet of the solar system.

- Because of the very low collisionality of most space and astrophysical plasmas, the shock thickness is determined by plasma processes.

- Even though the upstream and downstream regions can often be described using one-fluid MHD, the internal structure of the shock involves much smaller scales and therefore a fluidistic description like MHD cannot describe it properly.

- The image below shows the transverse structure of the Earth bow shock as observed by Cluster. The thickness is only a few electron inertial lengths (Schwartz et al 2011).

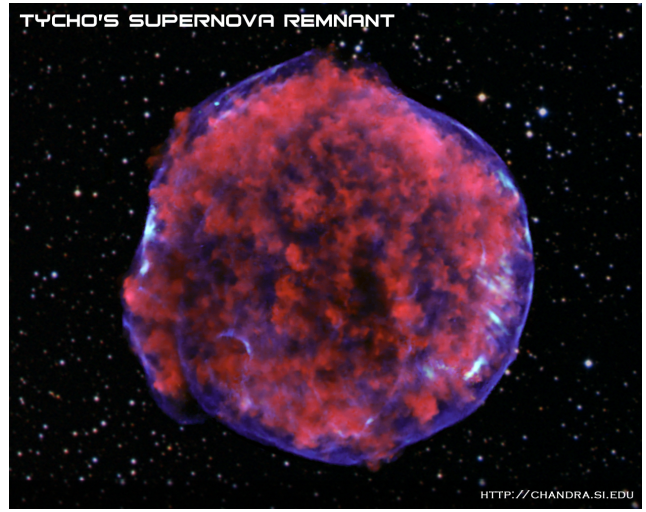

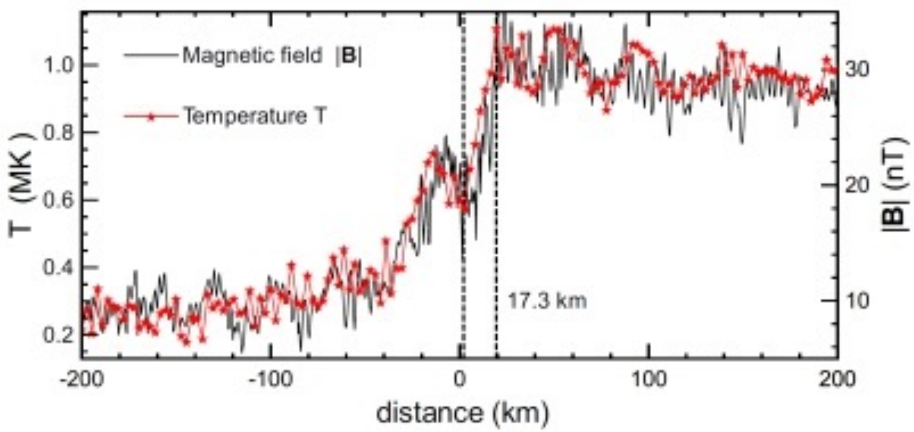

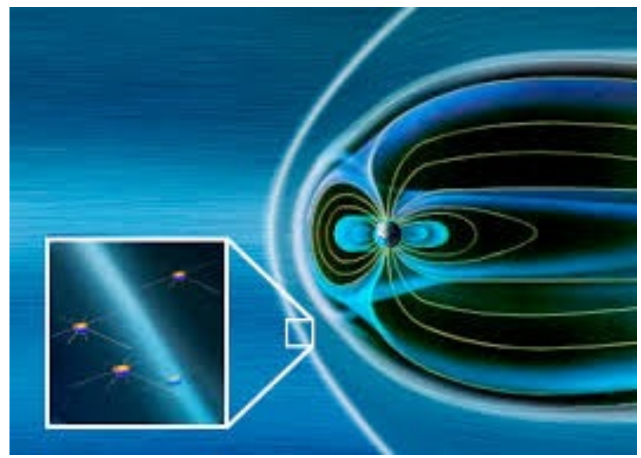

One dimensional two-fluid model

➡ We decided to use a two-fluid description to study the generation and propagation of perpendicular shocks.

➡ Perpendicular shocks correspond to the particular case where the magnetic field is tangential to the shock.

➡ We adopted a 1D version of the equations. All fields only vary in the direction across the shock (i.e. “x”).

➡ Tidman & Krall 1971 derive stationary solutions (solitons) for these same equations.

➡ Our two species are ions and electrons.

➡ Compressibility is essential for shock formation and dissipation is neglected.

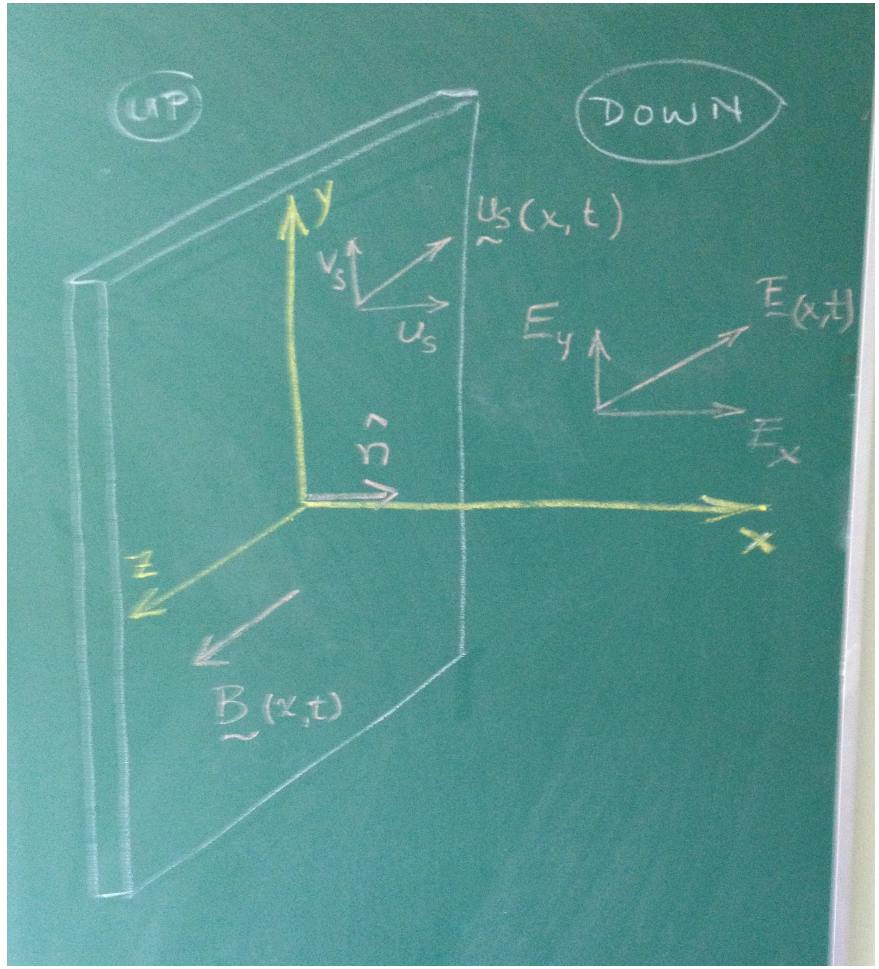

1D equations

- Note that $U_i=U_e=U$.
- As a result, the electrostatic potential can be obtained from the // Euler eqs.
- The perpendicular Euler equations predict that $m_e.V_e+m_i.V_i = \text{const}$, and we choose it equal to zero.
- The only linear mode propagating in a homogeneous background are fast magnetosonic waves.
- We integrate this set of 1D eqs. using a pseudo spectral code with periodic boundary conditions and RK2.
- The initial profile is a finite amplitude train of fast magnetosonic waves.
- Dissipation in these simulations is set to zero.

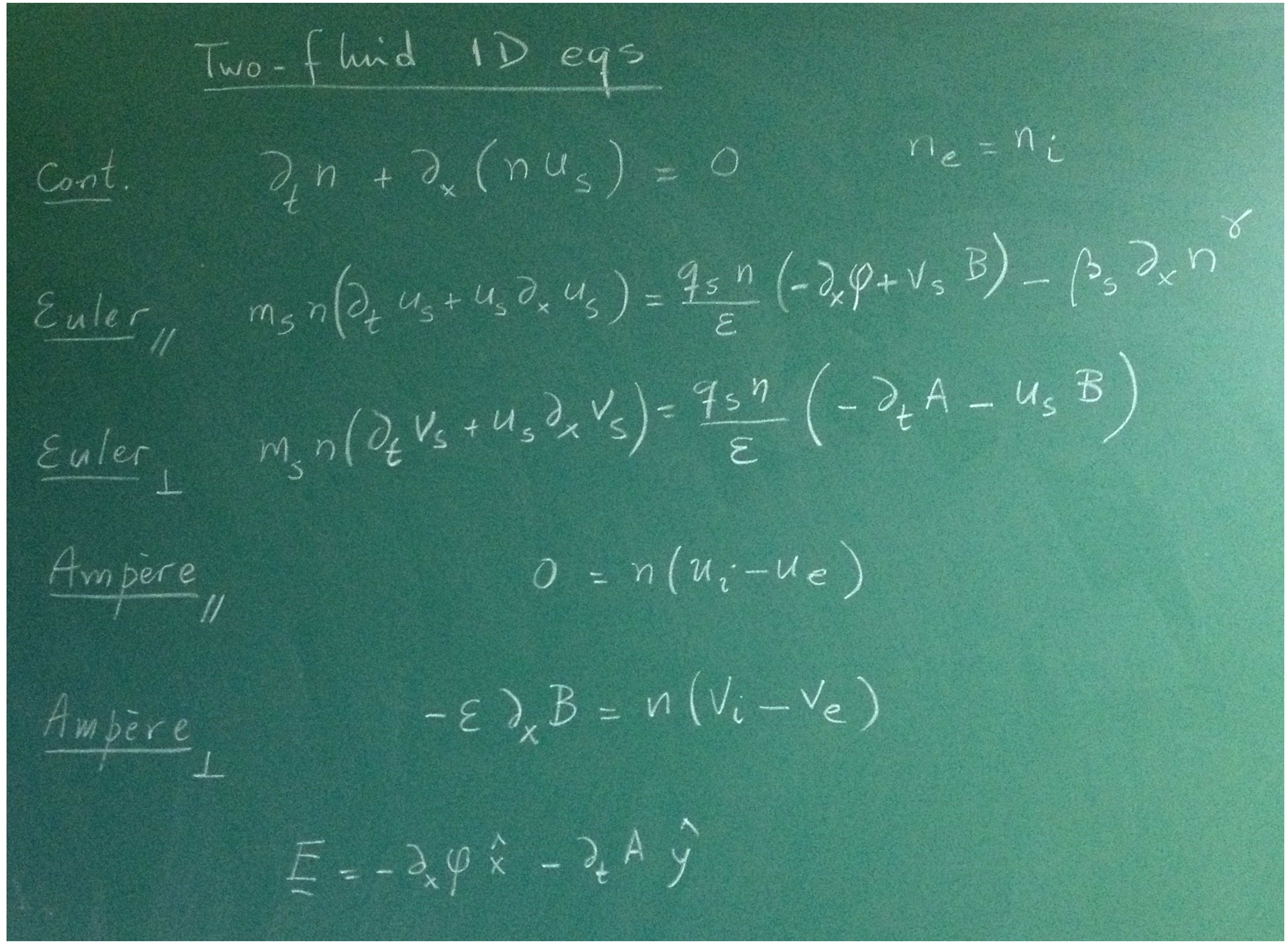

Shock formation

- We numerically integrate the 1D two-fluid equations to study the generation of the shock, internal structure and propagation properties (Gomez et al 2021).

- Our initial condition is a finite amplitude fast magnetosonic wave.

- The movie shows the evolutions of various profiles (parallel velocity, particle density and perpendicular magnetic field.

- Once the shock is formed, it propagates without distorsion.

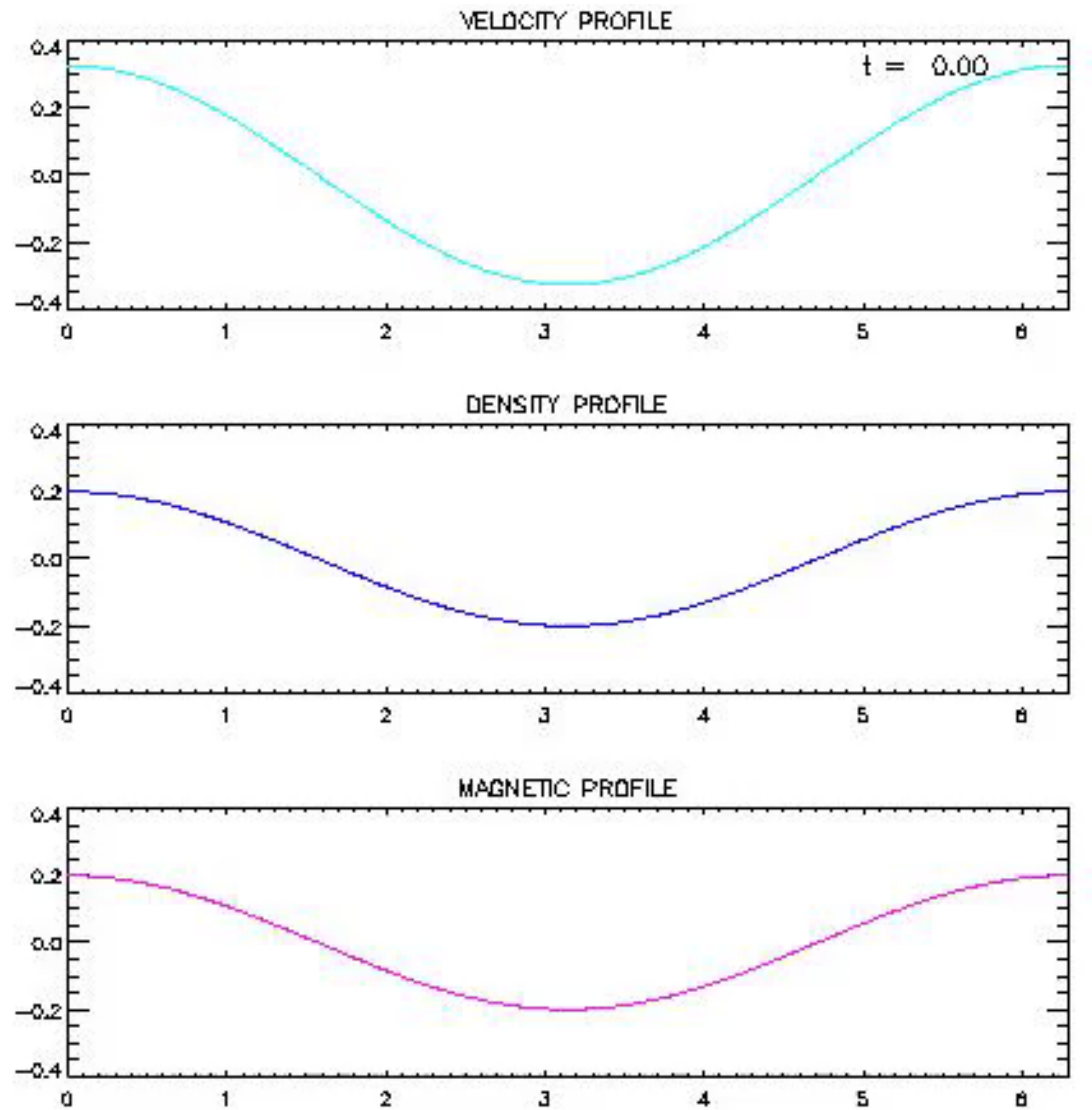

Shock profiles

- Once the shock is formed, we can study the transverse structure of the various relevant physical quantities.
- We can see the propagation of trailing waves in the downstream region, with wavelengths of a few electron inertial lenghts.
- Below we see the temporal evolution of the particle density profile. The initial profile is shown in light blue.

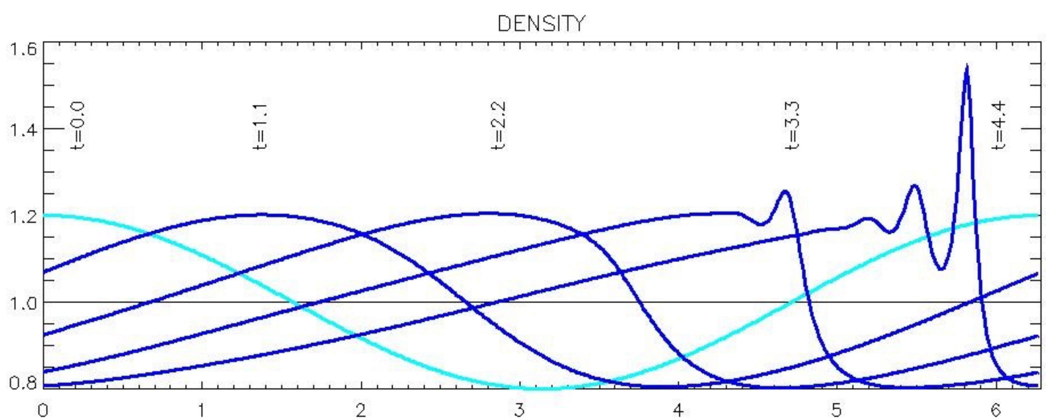

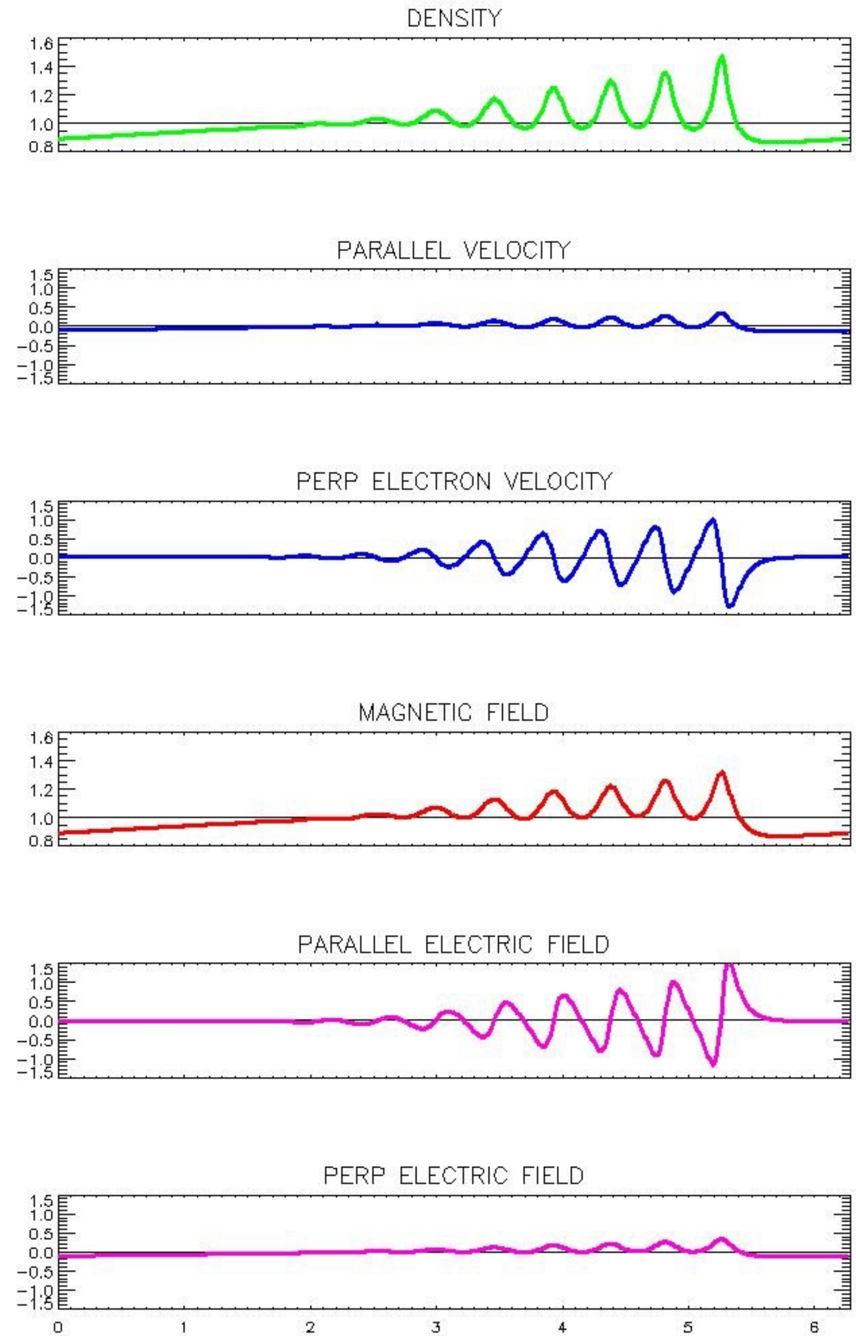

Ramp thickness

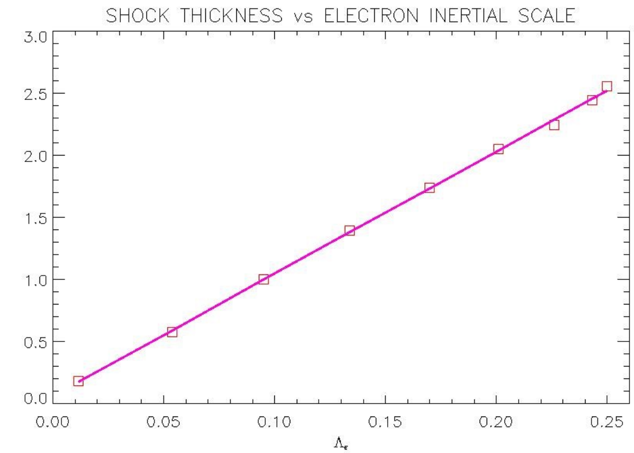

- We overlap the profiles U(x) for various runs with different mass ratios. In dark blue we show the ramp portion of each profile.
- We estimate the ramp thickness for each run and plot it against the corresponding electron inertial length. We find a perfect correlation, with ramp thicknesses of about ten electron inertial lengths.

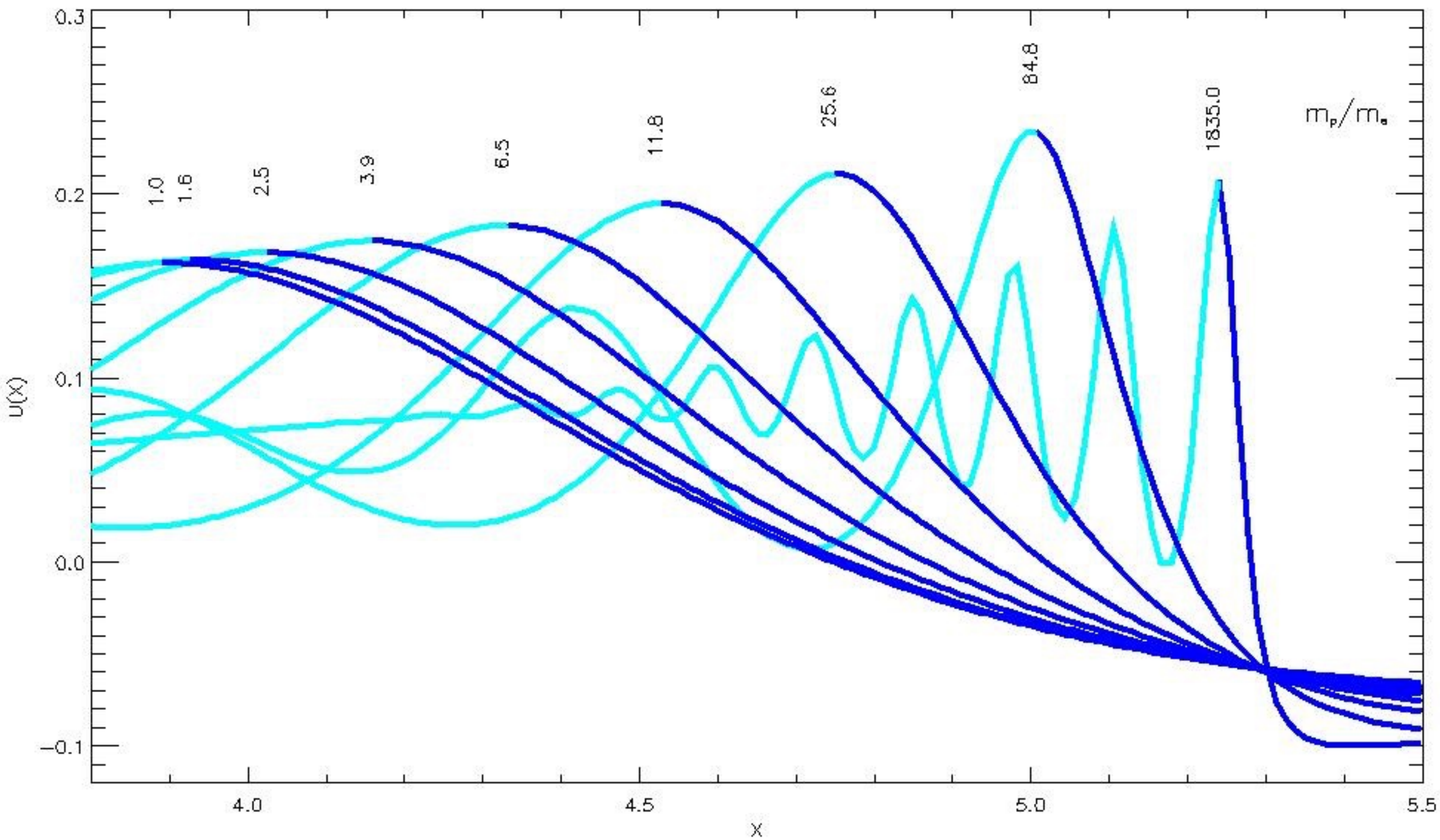

Magnetic reconnection

- The standard theoretical model for two-dimensional stationary reconnection is the so-called **Sweet-Parker model** (Parker 1958)

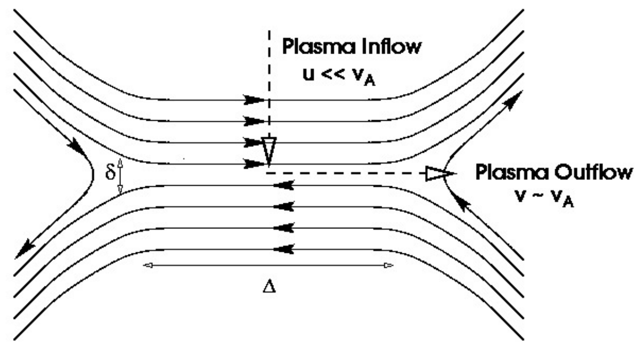

- It corresponds to a stationary solution of the MHD equations. The plasma inflow (from above and below) takes place over a wide region of linear size Δ and is much slower than the Alfven speed (i.e. $U_{in} << V_A$).

- The outflow occurs at a much thinner region (of linear size $\delta << \Delta$) at speed $U_{out} \sim V_A$.

- The efficiency of the reconnection process is measured by the so-called reconnection rate, which is the magnetic flux reconnected per unit time.

- The dimensionless reconnection rate is $$M = \frac{U_{in}}{U_{out}} \simeq S^{-1/2}$$

  where $S = \dfrac{\Delta v_A}{\eta}$ is the Lundquist number.

- Since for most astrophysical and space plasmas is S >> 1, the reconnection rate is exceedingly low.

Two-fluid simulations

➡ We perform simulations of the 2F-MHD equations in 2.5D geometry to study magnetic reconnection. We force an external field with a double hyperbolic tangent profile to drive reconnection at two X points (Andres et al. 2014a, PoP).

➡ We also study the turbulent regime of the 2F-MHD description, to look for changes at the electron skin-depth scale (Andres et al. 2014b, PoP).

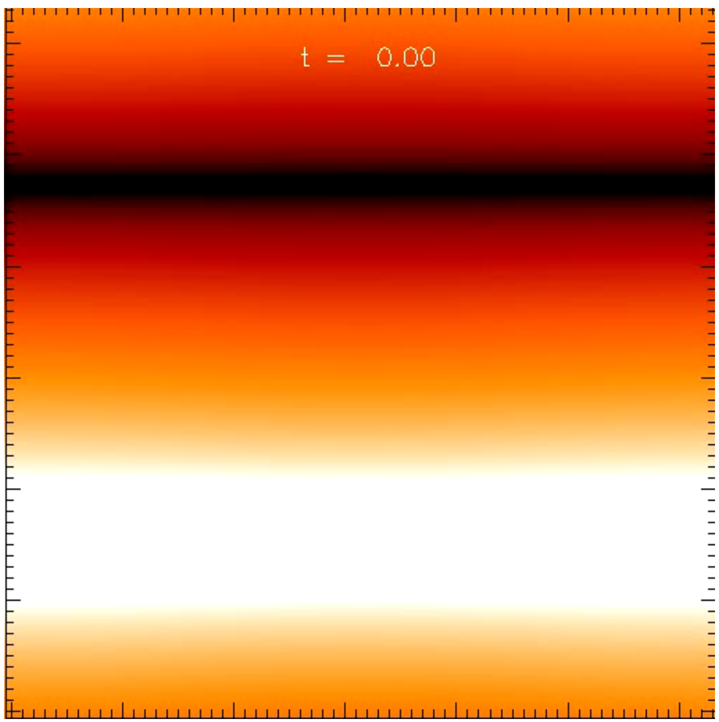

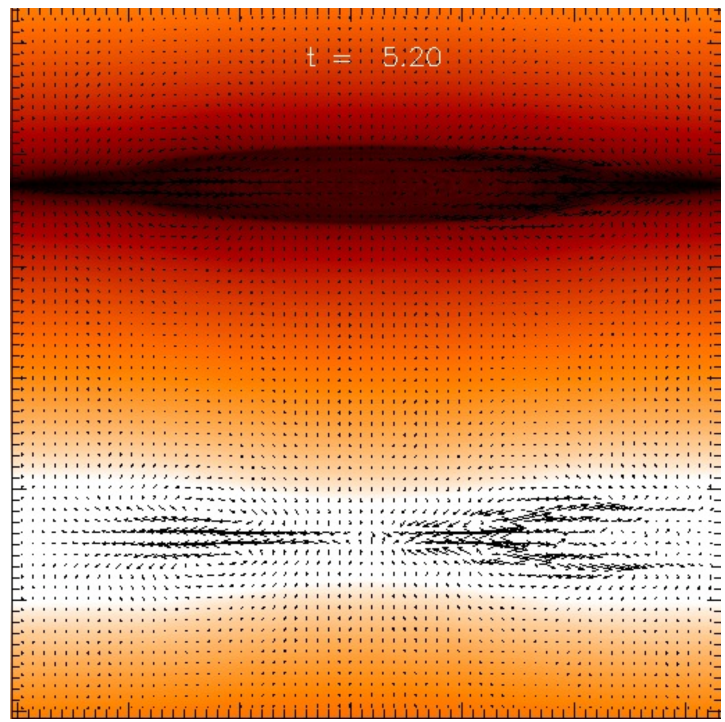

Two-fluid reconnection

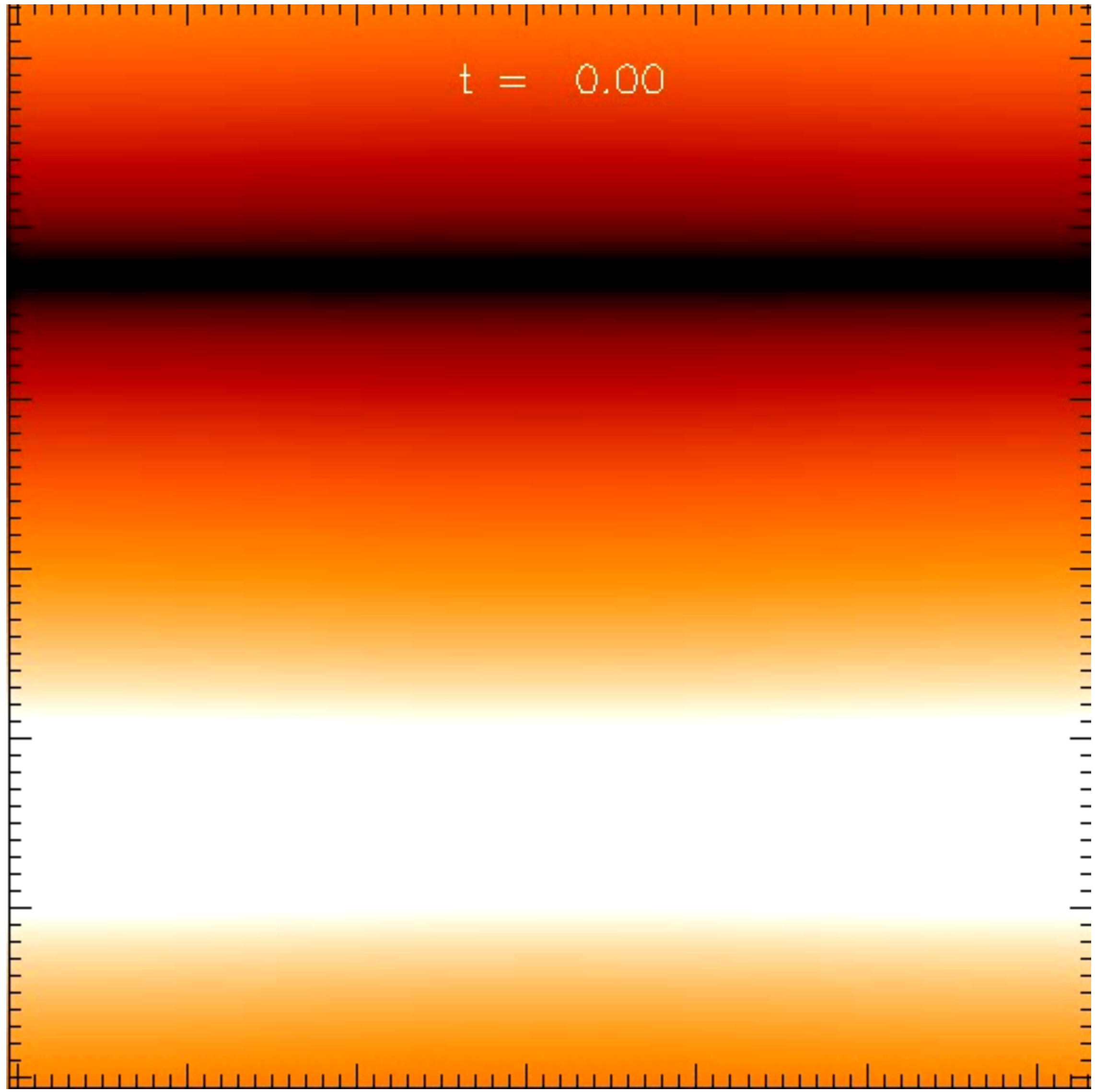

Two-fluid reconnection

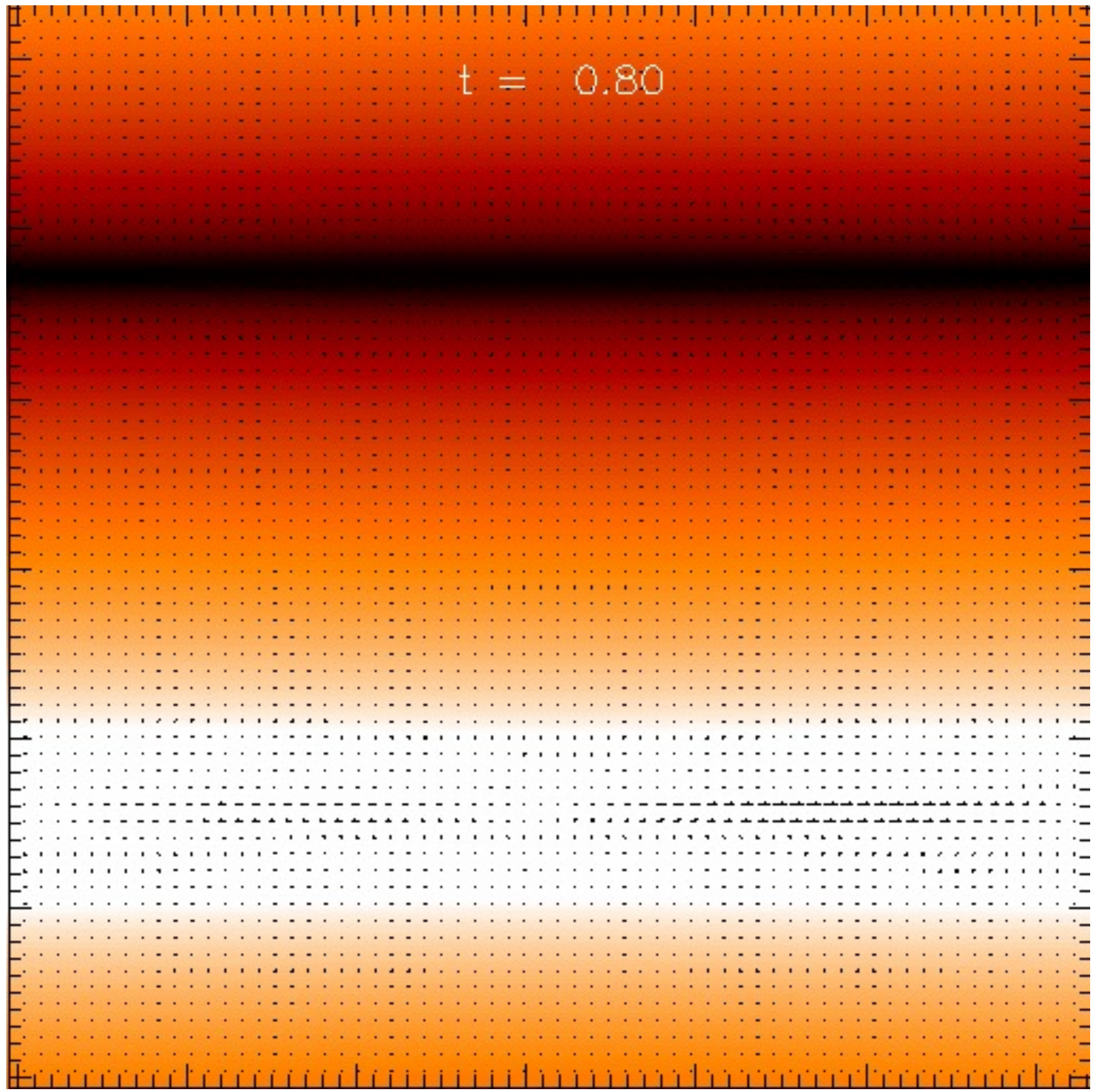

Two-fluid reconnection

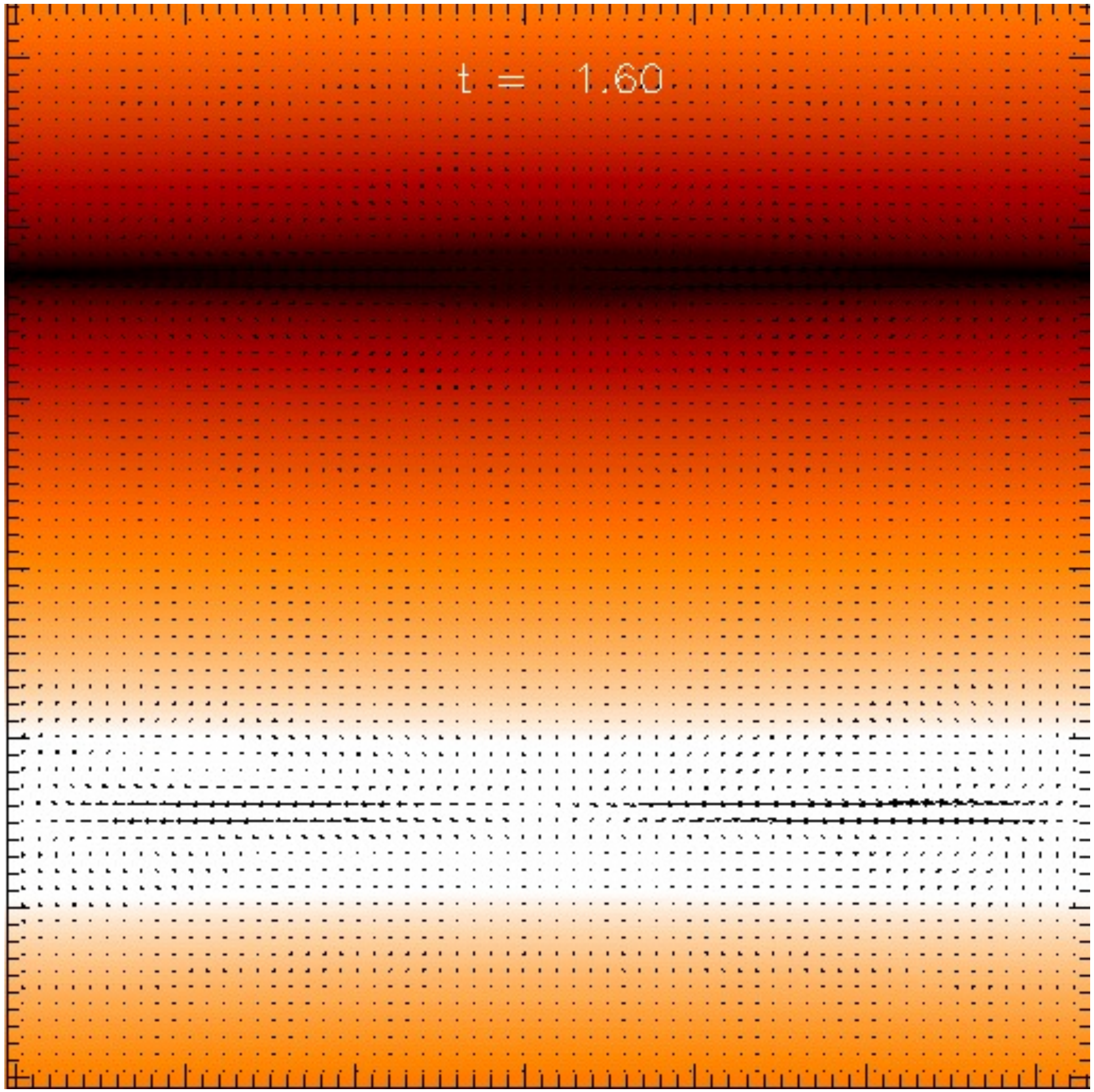

Two-fluid reconnection

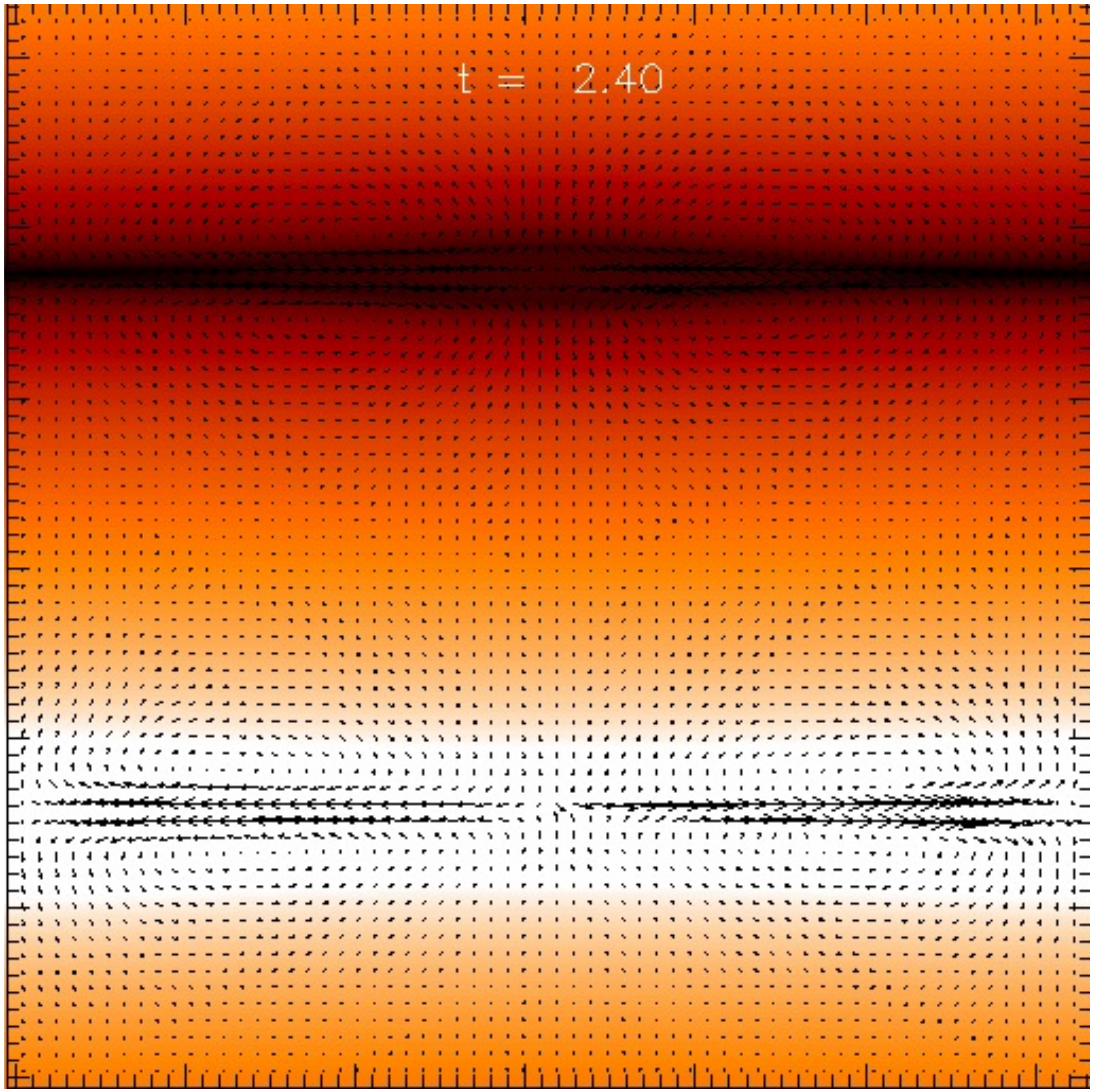

Two-fluid reconnection

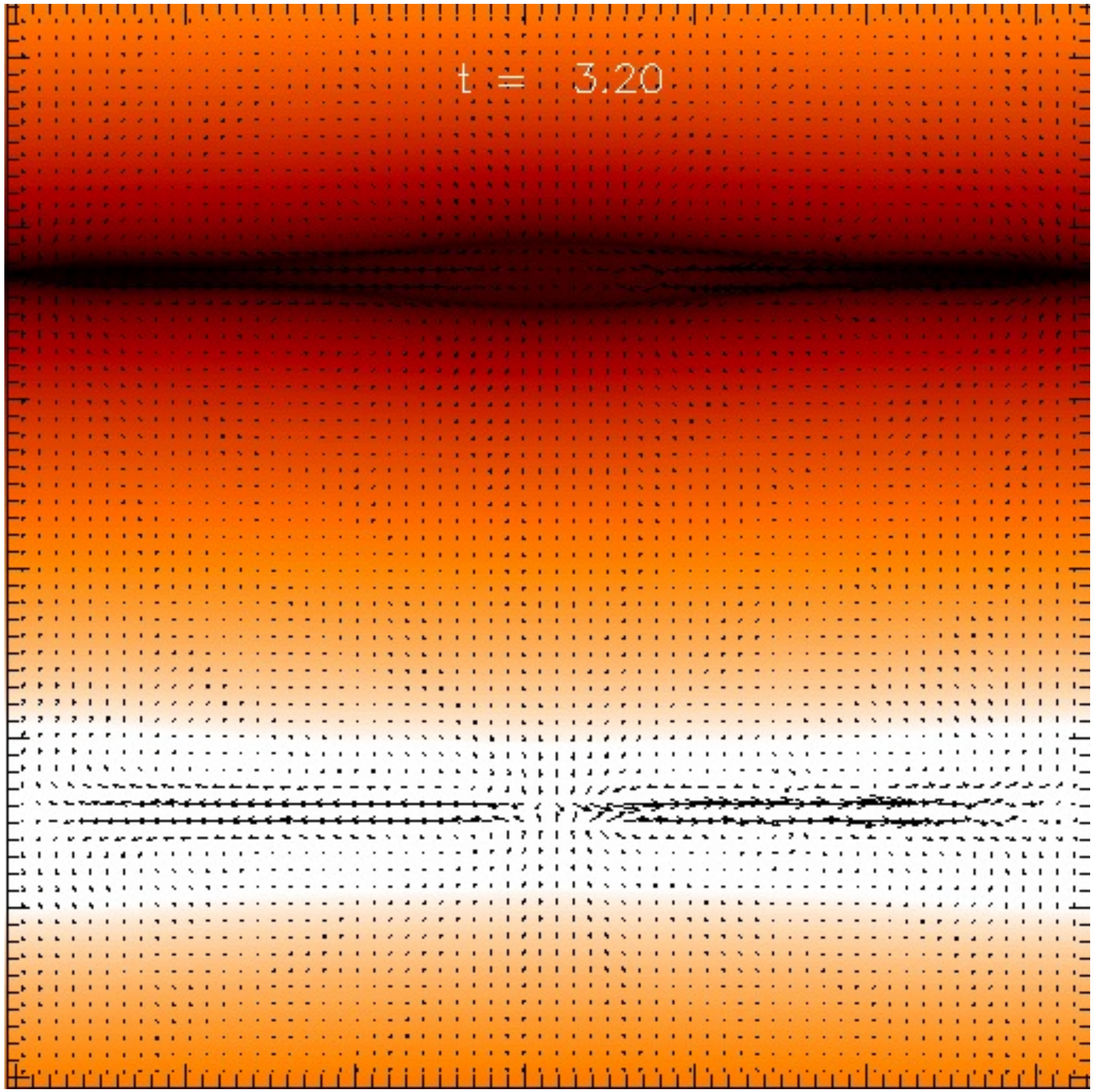

Two-fluid reconnection

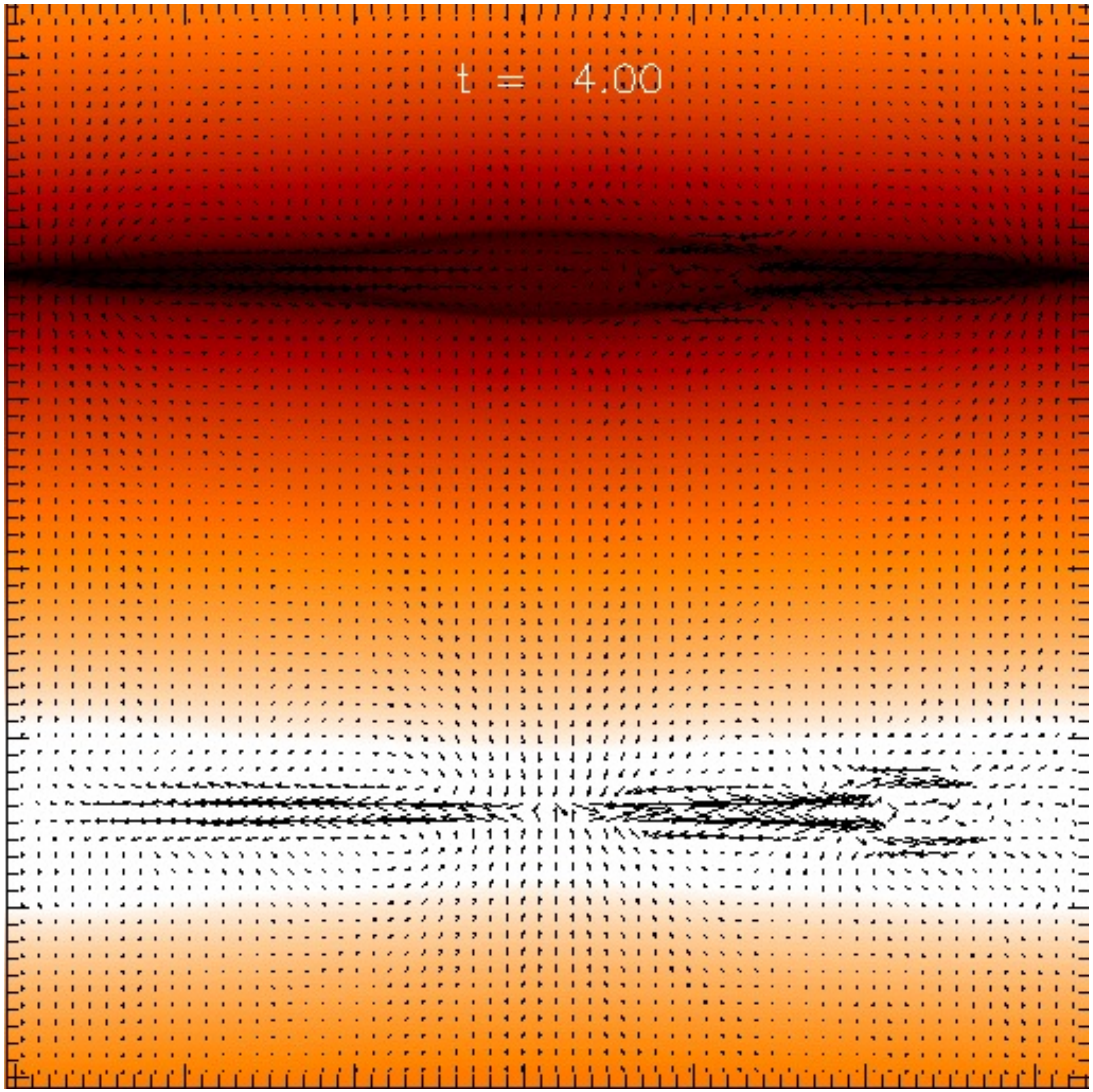

Two-fluid reconnection

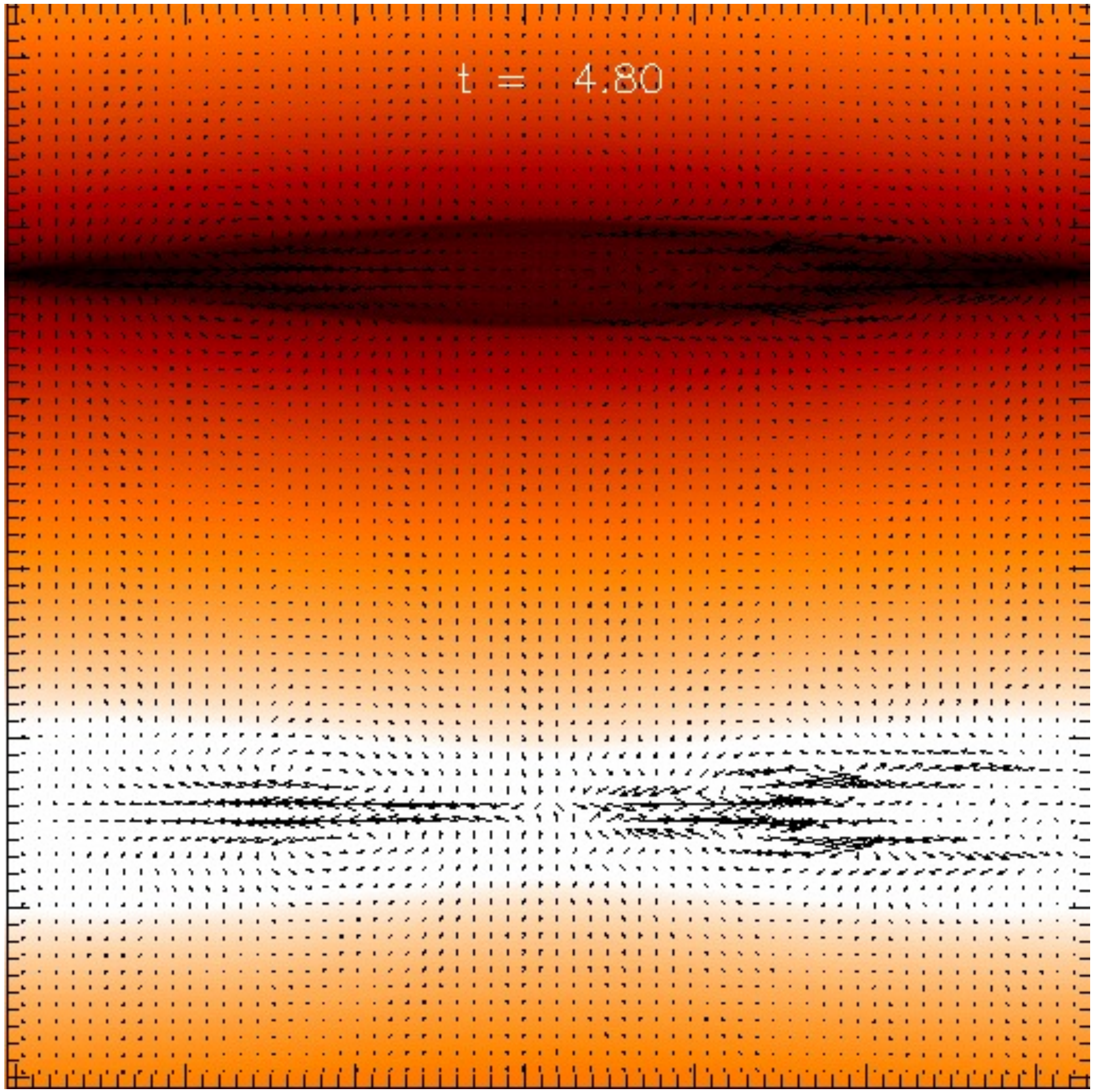

Two-fluid reconnection

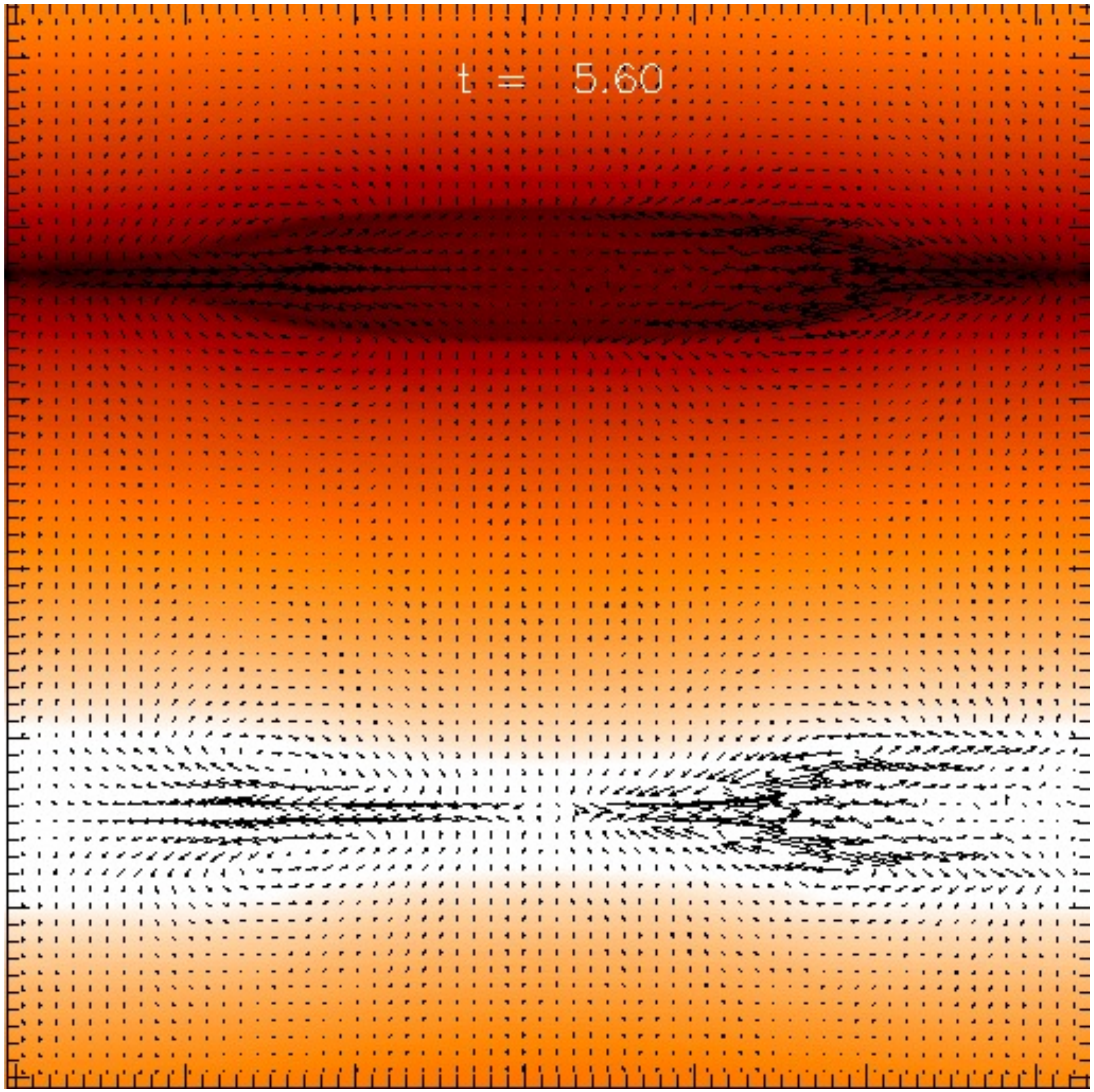

Reconnected flux in 2F-MHD

➡ The total reconnected flux at the X-point is the magnetic flux through the perpendicular surface that extends from the O-point to the X-point.

➡ We compare the total reconnected flux between a run that includes electron inertia and another one that does not.

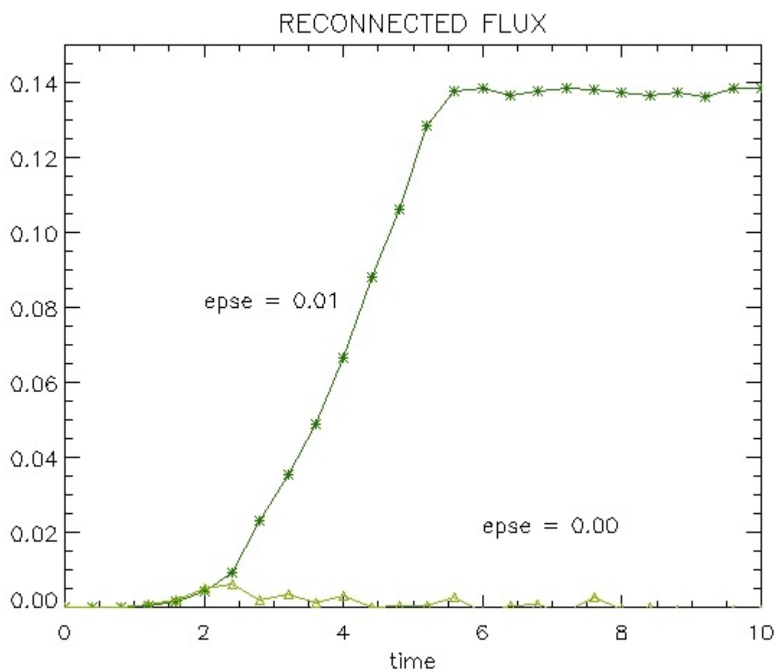

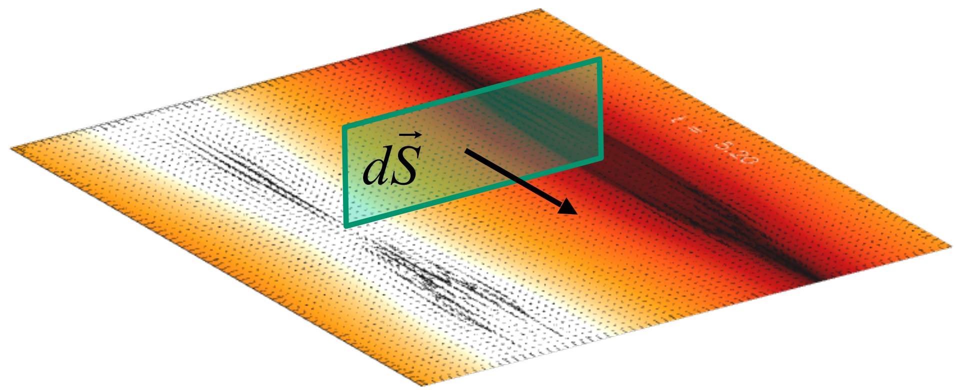

➡ The reconnection rate is the time derivative of these two curves.

➡ The apparent saturation is just a spurious effect stemming from the dynamical destruction of the X-point.

Reconnection rate in 2F-MHD

➡ For the 2D configuration and assuming incompressibility, we run several simulations with different values of the Hall parameter, which is the dimensionless ion inertial length.

➡ We compare the corresponding reconnected flux (above) and the reconnection rate (below) vs. time.

➡ The reconnection rate is E_z at the X-point. From the equation for electrons, under stationary conditions

$$E_z = -\frac{m_e}{e}\hat{z}\,.\,\vec{u}_e \times \vec{w}_e$$

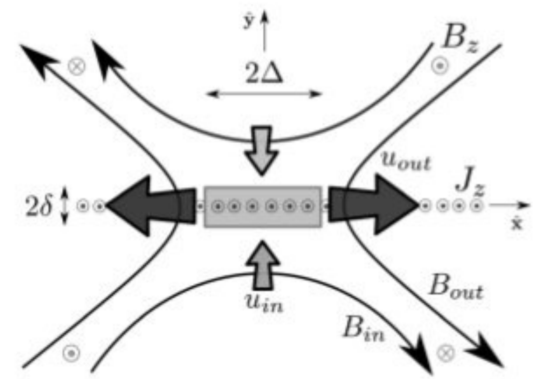

FIG. 1. Schematic 2.5D reconnection region.

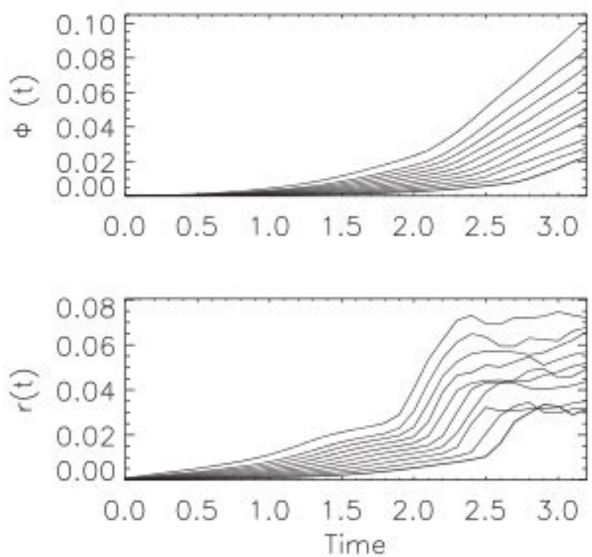

FIG. 3. Reconnected flux Φ (upper panel) and reconnection rate r (lower panel) as a function of time for $\lambda = 0.07, \ldots, 0.16$ (from bottom to top). For all runs, the electron to ion mass ratio is $m_e/m_i = 0.015$.

➡ At electron scales

$$\vec{u}_e \sim -\frac{1}{e\,n}\vec{j}$$

from where we obtain the following estimate for the dimensionless reconnection rate

$$R = \frac{c\,E_z}{B_0 v_A} \sim \frac{c}{w_{pi} L_0}$$

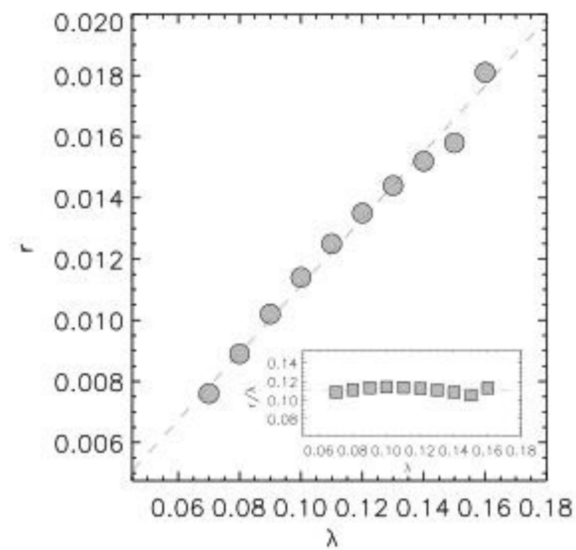

FIG. 6. Quasi-stationary reconnection rate r (gray circles) as a function of the Hall parameter λ. The best linear-fit for $\log \lambda - \log r$ is shown in gray-dashed line. Inset: Ratio between quasi-stationary reconnection rates and the Hall parameter (gray squares) as a function of the Hall parameter.

Turbulence in the Solar Wind

➡ The **solar wind** is a stream of plasma released from the upper atmosphere of the Sun, which impacts and affects the planetary magnetospheres.

➡ Sahraoui et al. 2009 used magnetograms from the Cluster mission to derive power spectra of magnetic energy.

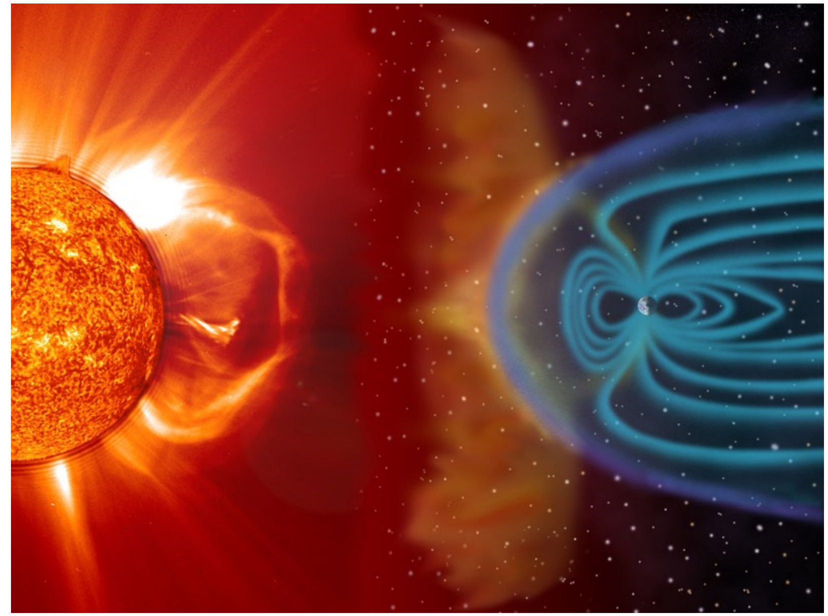

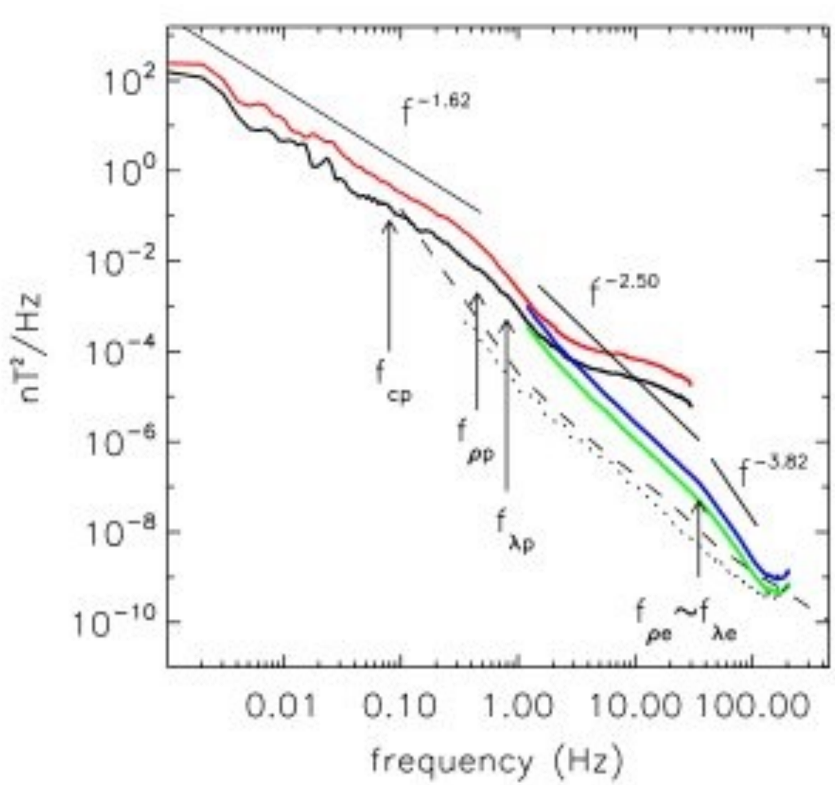

➡ They combine low-cadence data from FGM (**parallel** and **perpendicular** components) with high-cadence from STAFF-SC (also **parallel** and **perpendicular**).

➡ At the largest scales, they obtain a K41 power spectrum ($k^{-1.62}$).

➡ As they go to smaller scales, they identify two breakups. An intermediate range with a power law $k^{-2.50}$, and an even steeper range at the smallest scales ($k^{-3.82}$).

Turbulence in 2F-MHD simulations

➡ These breakups are a manifestation of physical effects beyond MHD.

➡ We performed incompressible 3072x3072 simulations of the full two-fluid equations. We excited a ring of large-scale Fourier modes and let the system relax while the turbulent energy cascade takes place (Andres et al. 2014b, PoP).

➡ The magnetic energy power spectrum shows two breakups at the approximate locations of the proton (k_p) and electron (k_e) scales.

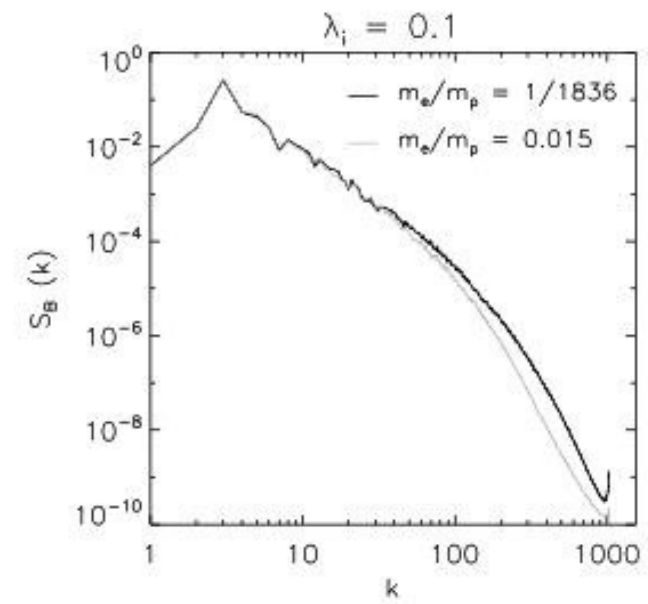

FIG. 1. Magnetic energy spectra for EIHMHD cases with $\lambda_i = 1/10$ and $m_e/m_p = 1/1836$ (black) and $m_e/m_p = 0.015$ (gray).

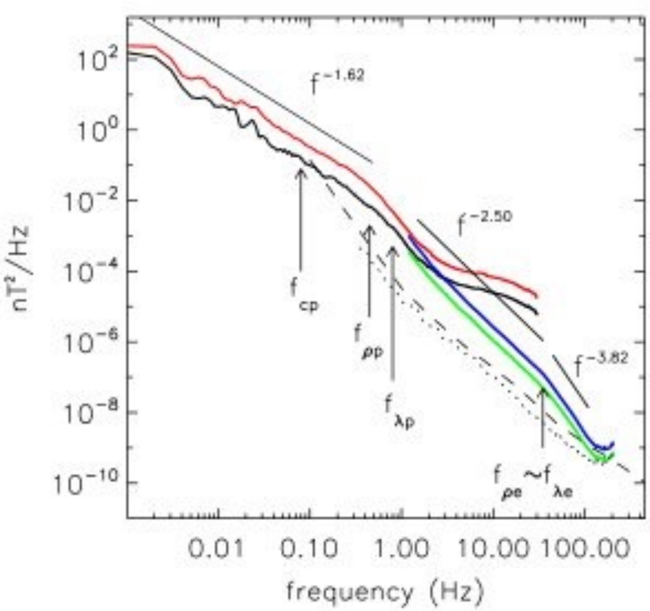

➡ The spectrum is K41 (i.e. $k^{-5/3}$) at $k << k_p$.

➡ At intermediate scales ($k_p << k << k_e$) is $k^{-7/3}$.

➡ Beyond the electron scale ($k_e << k$) a new range takes place $k^{-11/3}$.

➡ All these inertial ranges can be obtained using Kolmogorov-like arguments on the energy transfer rate given by

$$F_k \simeq k(u_k^3 + u_k B_k B_k' + (1-\delta)\lambda J_k B_k B_k' + (1-\delta)\delta\lambda^2 \partial_t J_k B_k).$$

Turbulence in 2F-MHD simulations

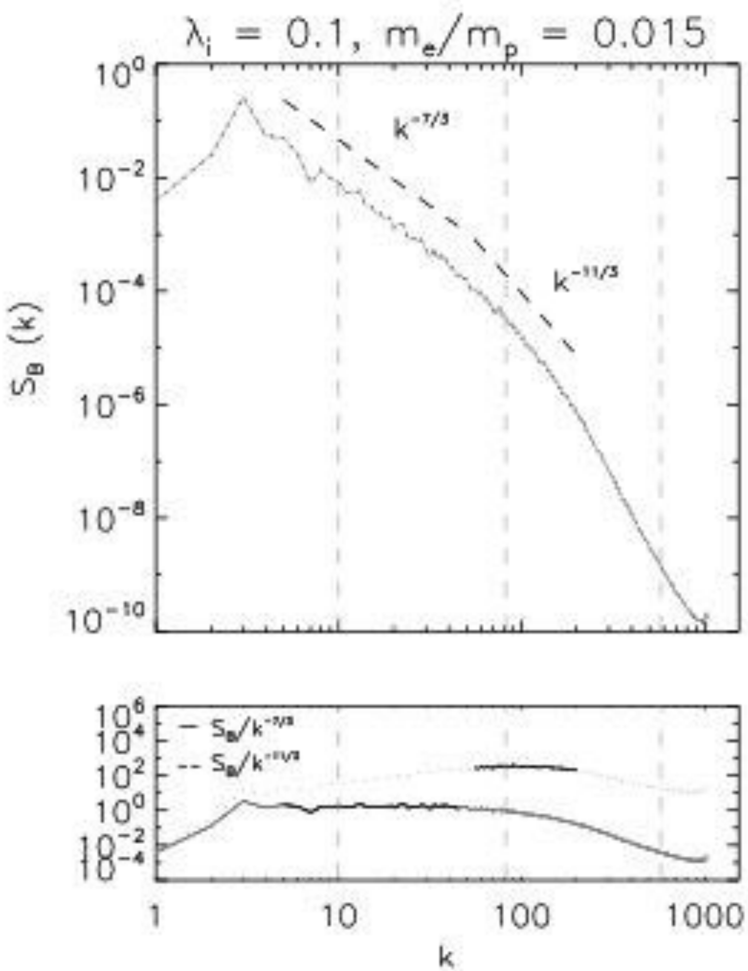

FIG. 2. Magnetic energy spectra for $m_e/m_p = 0.015$. Vertical dashed gray lines correspond to $k_{\lambda_i} \sim 10$, $k_{\lambda_e} \sim 82$, and $k_{\rho_e} \sim 550$. The compensated spectrum for the HMHD (solid line) and EIHMHD (dashed line) regions are shown in the lower panel.

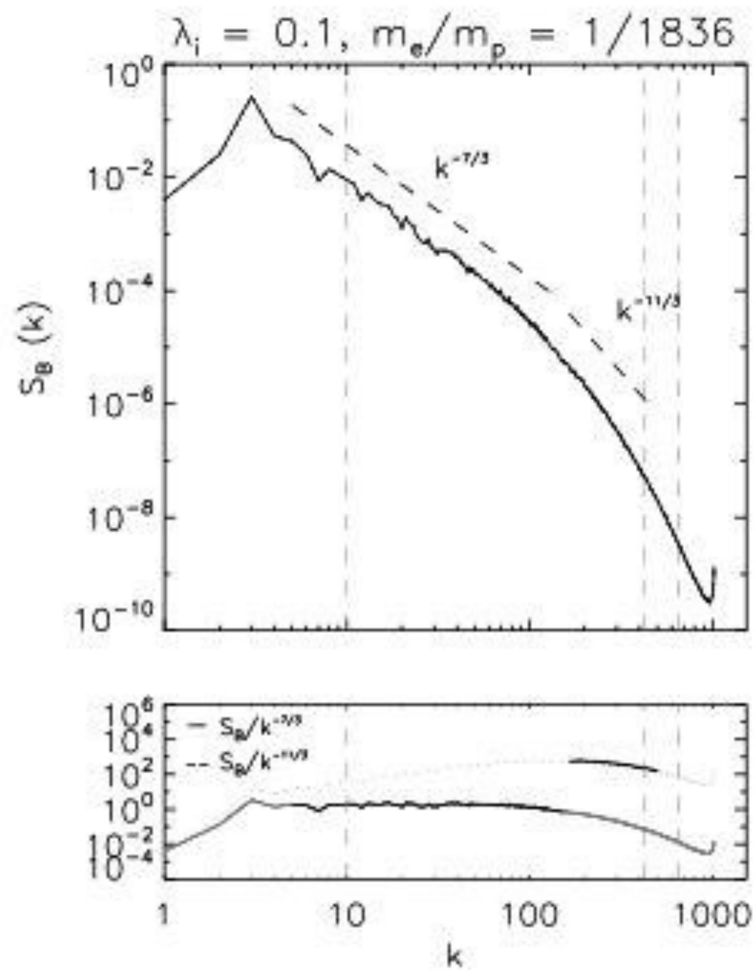

FIG. 3. Magnetic energy spectra for $m_e/m_p = 1/1836$. Vertical dashed gray lines correspond to $k_{\lambda_i} \sim 10$, $k_{\lambda_e} \sim 430$, and $k_{\rho_e} \sim 650$. The compensated spectrum for the HMHD (gray line) and EIHMHD (green line) regions in the same format as Figure 2.

Conclusions

- **One-fluid MHD** is a reasonable theoretical framework to describe the large-scale dynamics of plasmas.

- **Two-fluid MHD** introduces new physics (Hall, electron pressure, electron inertia) and also new spatial scales, such as the proton and electron inertial lengths. We studied the role of these plasma effects on three relevant phenomena for astrophysical and space plasmas: **shocks**, **reconnection** and **turbulence**.

- **Shocks**:
  1D simulations show that a train of fast magnetosonic waves decay into a train of shocks. Thickness is a few times the electron inertial scale.

- **Reconnection**:
  Our 2F-MHD simulations show fast magnetic reconnection without energy dissipation (Andres et al. 2014a, PoP). The reconnection rate scales like the ion inertial scale and is independent from the electron mass.

- **Turbulence**:
  Externally driven 2F-MHD runs show turbulent regimes. The magnetic energy spectrum displays breakups at the ion and electron inertial scales (Andres et al. 2014b, PoP). Spectral slopes can also be obtained by dimensional analysis.

Induced magnetospheres

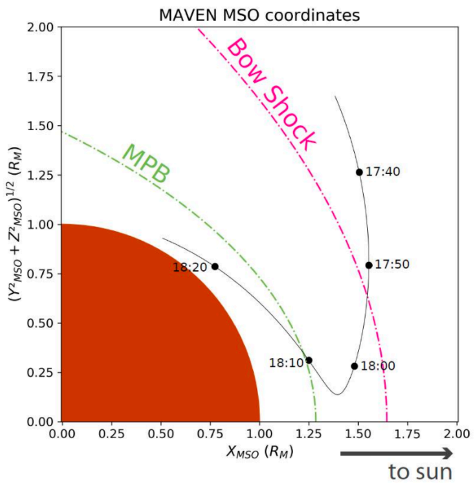

Figure 1. Geometry of MAVEN orbit 2844 between 17:40 and 18:20 UTC in cylindrical MSO coordinates. The orbit is shown in black and the mean position of the bow shock and MPB (Vignes et al., 2000) in magenta and green respectively.

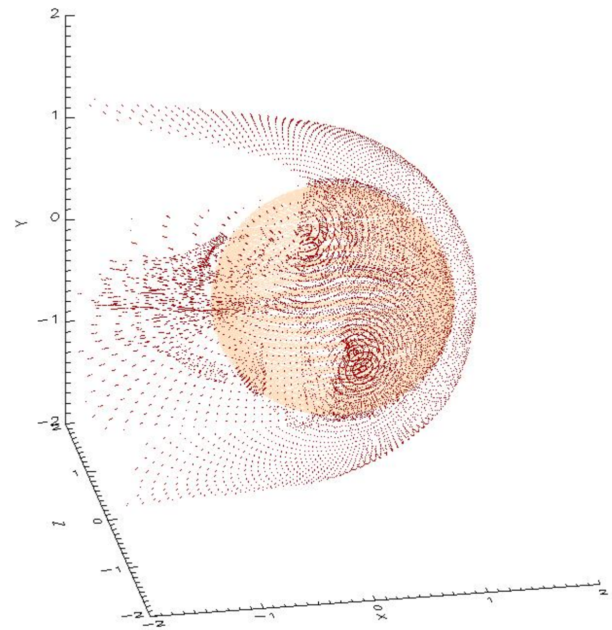

- Planetary magnetospheres form because of an equilibrium between the local magnetic field and the solar wind ram pressure.
- Planets like Mars or Venus do not have magnetic fields. The interaction is between the wind and the planetary ionospheres.
- A transition region or **magnetic pileup boundary** (MPB) is formed beyond the downstream region.
- We ran 3D multifluid simulations in collaboration with Dong (Dong et al. 2014, GRL).
- It includes protons, several ionospheric ions, and massless electrons.
- The picture shows the region where the plasma beta equals unity to identify the MPB.

Magnetic pileup boundary

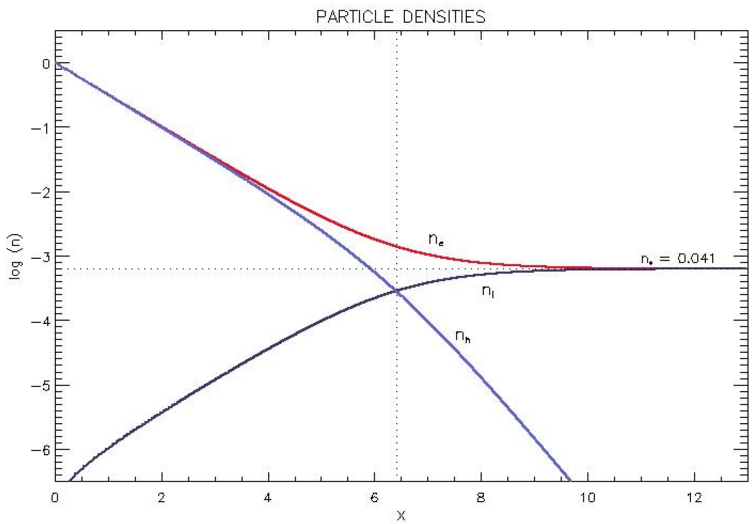

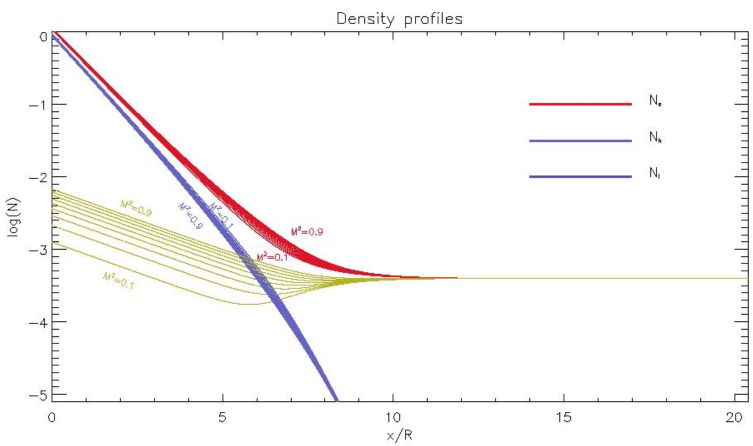

- A nice analytical exercise is to assume B=0 and look for 1D stationary solutions for a plasma made of three species:

  p: protons
  e: electrons
  h: heavy ions

- To the right, we have the solar wind made of a fully ionized hydrogen plasma.

- To the left, above of the planetary surface, we have a static and gravitationally stratified atmosphere, made of singly charged heavy ions (such as O+, O2+, CO+ and CO2+).

- In between, electrons satisfy electric charge quasi-neutrality, as observed in the picture.

- In the picture below, the density profiles for different values of the Mach number are shown.

- To the right of this transition, we have a shocked, subsonic solar wind. To the left, we have a static ionosphere.

- When we include the magnetic field, fieldlines carried by the solar wind remain frozen to the electrons and pile-up in front of the much denser ionosphere.

Magnetic pileup boundary

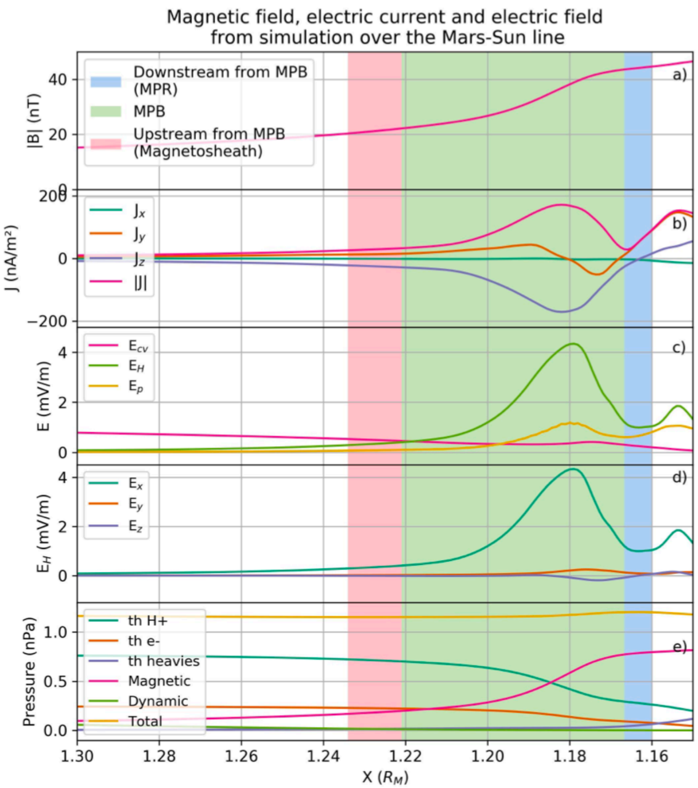

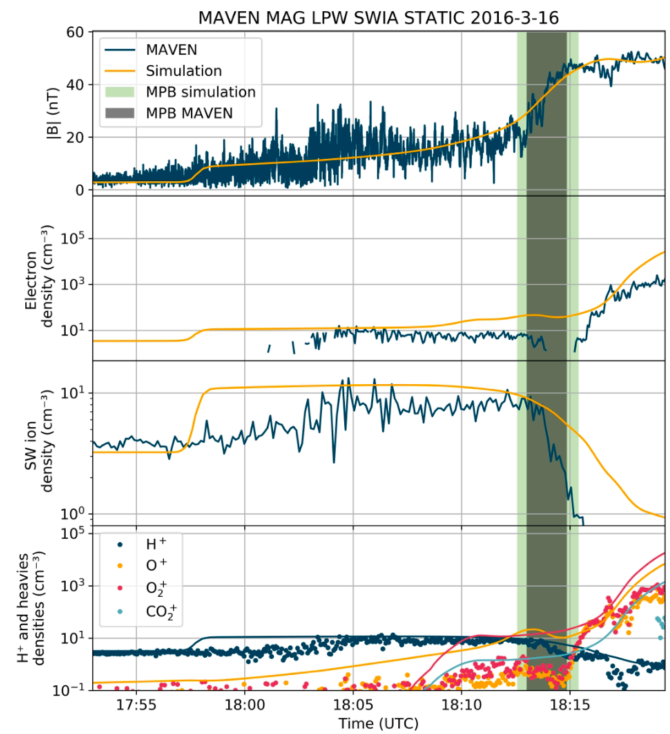

Figure 5. Comparison of MAVEN data and the simulation results over the trajectory. From top to bottom: Magnetic field magnitude. Electron density (LPW values for densities greater than 1 cm^{-3}). Solar wind ion density (proton density only for simulation data). Ion density of different species (H+, O+, O2+, CO2+), STATIC data is represented by dots and simulation data is the continuous line. The MPB from simulation data is shaded in green and from MAVEN data is shaded in grey.

Figure 6. Simulation results on the $\hat{x}$ axis. From top to bottom: (a) Magnetic field strength. (b) Volume current density components and strength. (c) Magnitude of the convective, Hall and pressure gradient electric fields. (d) Hall electric field components. (e) Different pressures, as indicated. The bow shock (not depicted) is at approximately 1.5 R_M.